Asian Jet Waveguide and a Downstream Extension of the North Atlantic Oscillation

MASAHIRO WATANABE

Division of Ocean and Atmospheric Science, Hokkaido University, Sapporo, Hokkaido, Japan

(Manuscript received 18 July 2003, in final form 10 February 2004)

ABSTRACT

Anomalous atmospheric fields associated with the North Atlantic Oscillation (NAO) are analyzed on interannual and intraseasonal time scales in order to examine the extent to which the NAO is a regional phenomenon.

Analyses on the interannual time scale reveal that the NAO signal is relatively confined to the Euro–Atlantic sector in December while it extends toward East Asia and the North Pacific in February. The difference is most clearly seen in the meridional wind anomaly, which shows a wave train along the Asian jet, collocated with an anomalous vorticity source near the jet entrance. Diagnoses using a linear barotropic model indicate that this wave train is interpreted as quasi-stationary Rossby waves trapped on the Asian jet waveguide, and effectively excited by the anomalous upper-level convergence over the Mediterranean Sea. It is found that, when the NAO accompanies the Mediterranean convergence (MC) anomaly, most frequently seen in February, the NAO indeed has a much wider horizontal structure than the classical picture, rather similar to the Arctic Oscillation. In such cases interannual variability of the NAO is tied to the East Asian climate variability such that the positive NAO tends to bring a surface warming over East Asia.

Similar results are obtained from an analysis of individual NAO events based on low-pass-filtered daily fields, which additionally identified that the downstream extension occurs at the decay stage of the NAO event and the MC anomaly appears to be induced by the Ekman pumping associated with the NAO. The signal of the MC anomaly can be detected even at 5 days before the peak of the NAO, suggesting that the NAO influence to East Asia is predictable to some extent; therefore, monitoring the developing NAO event is useful to the medium-range weather forecast in East Asian countries.

1. Introduction: AO or NAO?

Atmospheric low-frequency variability, often called the teleconnection pattern, has long been one of the major targets in studies for large-scale weather and climate variations. In particular, the North Atlantic Oscillation (NAO), which has been identified many decades ago (Walker and Bliss 1932; van Loon and Rogers 1978; Wallace and Gutzler 1981; Barnston and Livezey 1987), is focused on during recent years in order to understand its dynamical origin, regional impact, and causes for the fluctuations on decadal to centennial time scales.

One of the reasons why the NAO is actively reexamined is the Thompson and Wallace (1998, 2000) work, which advocated a presence of the principal mode of variability that consists of hemispheric-scale anomalies in sea level pressure (SLP) or geopotential height fields, referred to as the Arctic Oscillation (AO). Since the anomalies associated with the AO over the North Atlantic considerably resemble those associated with the NAO and, indeed, indices for these two are highly correlated, the proposal of the AO concept gave rise to confusion about the relationship between the NAO and AO, namely, which phenomenon would be more adequate in understanding the atmospheric low-frequency variability. Since the AO is defined by the leading empirical orthogonal function (EOF) of the wintertime monthly SLP anomalies (Thompson and Wallace 1998), which automatically tends to favor the largest scale of patterns that best explain the hemispheric covariance, several studies point out some doubt of its physical relevance by showing a lack of temporal coherence between the atmospheric anomalies over the Pacific and Atlantic sectors associated with the AO (Deser 2000; Ambaum et al. 2001; Monahan et al. 2001; Itoh 2002). While these studies suggest the traditional NAO being more adequate than the AO, there are also counterarguments (Wallace and Thompson 2002; Christiansen 2002), therefore this issue is still controversial.

As part of the above debate, it seems that the NAO is recognized as a regional mode of variability, in contrast to the AO that emphasizes a hemispheric-scale spatial coherence. Thus the controversy may also be interpreted as a question whether the principal low-frequency modes of the dynamical atmosphere have a regional scale or a hemispheric scale. On the other hand, it is known that the NAO, which is indeed regional in the SLP field, accompanies hemispheric-wide surface tem-

Corresponding author address: Dr. M. Watanabe, Division of Ocean and Atmospheric Science, Hokkaido University, Nishi 5, Kita 10, Sapporo, Hokkaido 060-0810, Japan.
E-mail: hiro@ees.hokudai.ac.jp

perature anomalies, in particular over Eurasia (Hurrell 1995, 1996; Xie et al. 1999). In addition, a recent work by Branstator (2002, hereafter B02) shows that a set of zonally oriented circulation anomalies along the Asian jet stream emerges in concert with the NAO, though it is found only on the intraseasonal time scale. Given these observational results, this study aims to clarify the extent to which the NAO is actually regional. Since the NAO pattern is known to dominate on multiple time scales, we will examine the above question on two different time scales: interannual and intraseasonal bands. The former time scale, in which the NAO has larger variance (Kushnir and Wallace 1989; Feldstein 2000), can be discussed with monthly mean observations as in the literature (van Loon and Rogers 1978; Wallace and Gutzler 1981) while the latter with daily fields. Even though the teleconnection patterns such as the NAO have been identified as the most persistent, recursive circulation anomalies, therefore alternatively called persistent anomalies (Dole and Gordon 1983), weather regimes (e.g., Kimoto and Ghil 1993), and growth/decay life cycles (Feldstein 2003), all of these studies point out relatively short decorrelation time of individual *events* of less than 2 weeks. The NAO signature found on the interannual time scale may thus be a stochastic representation of those events, leading to an expectation that similar features on which we focus are detected both in monthly and daily fields if we can assume no specific external forcing such as the tropical heating strongly affecting the interannual variability of the NAO.

By means of a simple linear regression analysis to observed monthly anomalies, we show that the NAO does have a wider horizontal scale in a certain month, contributing to high correlation with the AO index during that period. The nearly hemispheric scale of the NAO is due to a downstream extension toward East Asia and the North Pacific by a zonally oriented pattern in circulation anomalies, which appears the same as the ''circumglobal teleconnection'' described in B02. Such a pattern in monthly mean fields can be interpreted as quasi-stationary Rossby waves on the Asian jet waveguide (Hoskins and Ambrizzi 1993), so we then use a linear barotropic model to detect vorticity sources that effectively excite the Rossby waves and hence link the NAO signal over the Atlantic with the downstream circulation anomalies. Composite analysis to daily, low-pass filtered anomalies reveals finer temporal evolution of the downstream extension of the NAO, in which the circumglobal pattern is established during 2–4 days following the peak of the NAO. Propagation of wave packets, but not the wave itself, on the Asian jet is quite evident in the daily anomalies, indicating that the Rossby wave argument appears relevant for individual NAO events as well, although the anomalies are not stationary anymore.

In section 2, observational data and a barotropic model are described. Monthly mean fields are analyzed in section 3, in which the interannual variability of the NAO is investigated and compared during winter months, demonstrating that the eastward extent of the circulation anomalies associated with the NAO varies month by month. Also in section 3, dynamics responsible for the eastward extension of the NAO is examined by means of linear barotropic model diagnosis. Both observational and numerical analyses suggest a vital role of the anomalous upper-level convergence over the Mediterranean Sea in leading to the downstream extension of the regional NAO signal. Daily mean fields are then used in section 4 in order to verify that those processes are indeed identified in intraseasonal NAO events. Conclusions and some remarks are finally presented in section 5.

2. Data and model

a. Observational data

Observed atmospheric fields used in this study are derived from the National Centers for Environmental Prediction–National Center for Atmospheric Research (NCEP–NCAR) reanalysis (Kalnay et al. 1996), which spans from January 1948 to December 2002. Most of the data are available on a $2.5^\circ \times 2.5^\circ$ grid at standard pressure levels.

For monthly mean fields, the monthly climatology was first subtracted for each variable and deviations from the climatology; that is, anomalies are used in the analysis. Since the AO/NAO is prevailing in boreal winter, we mainly focus on the monthly anomalies from December to February. The anomalies on interannual time scale associated with the NAO and AO are obtained by linear regressions onto the monthly indices for the NAO and the AO, respectively. The NAO index is a conventional one, defined by a normalized SLP difference between Lisbon, Portugal, and Stykkisholmur, Iceland, (Hurrell 1995) while the AO index is adopted from the principal component associated with the leading EOF of the monthly 1000-hPa height (equivalent to SLP) anomaly, provided by the Climate Prediction Center. Regressed anomalies corresponding to one standard deviation of each index are hereafter referred to as either the monthly NAO or AO anomalies.

As for daily average fields, the climatology is defined by a 55-yr mean value for each calendar day, then daily anomalies are obtained as in the monthly anomalies. A four-pole, Butterworth low-pass filter, which retains periods longer than 10 days, is applied to daily anomalies in order to remove transient synoptic disturbances. Then the EOF analysis is performed on the filtered SLP anomalies over the Atlantic sector of 20°–90°N, 120°W–30°E during 1 November through 30 April in order to extract the NAO signature in the daily low-frequency fields. As will be shown in section 4, the leading EOF well represents the NAO pattern, and the associated principal component (referred to as the PC1) reveals quite high

coherence with the conventional NAO index such that the correlation coefficient of the December–February average of this PC1 time series with the Hurrell index exceeds +0.87. All analyses of daily filtered data are made with PC1 as a reference time series. While variables that we analyze contain upper-level irrotational and nondivergent flow fields as calculated from the velocity potential and streamfunction on a sigma surface in addition to geopotential height and zonal and meridional winds at pressure levels, only some of them are presented in the present paper.

b. Barotropic model

The model follows a barotropic vorticity equation linearized about the observed 300-hPa climatological flow, as expressed by

$$\partial_t \nabla^2 \psi' + J(\overline{\psi}, \nabla^2 \psi') + J(\psi', \nabla^2 \overline{\psi} + f) + \alpha \nabla^2 \psi' + \nu \nabla^6 \psi' = S', \quad (1)$$

where J denotes a Jacobian operator and $\overline{\psi}$ and ψ' are respectively the basic state and perturbation streamfunctions; f is the Coriolis parameter, while an anomalous vorticity source induced by the divergent part of the circulation is symbolically represented by S'. The model includes a linear damping that represents the Rayleigh friction and a scale-selective biharmonic diffusion. The coefficient ν is determined such as to damp the smallest-scale eddy in 1 day while the coefficient α is set at $(10 \text{ days})^{-1}$, which ensures that the system is marginally stable.

Equation (1) can be solved with a given S' on a spherical domain in which the perturbation streamfunction is represented by spherical harmonics of T42 horizontal truncation.

3. Interannual variability

As mentioned in the introduction and also reported in many articles (e.g., Deser 2000; Wallace 2000; Ambaum et al. 2001; Kodera and Kuroda 2003), winter NAO and AO indices are highly correlated although the former (latter) is thought to represent a regional (hemispheric) pattern of variability. Before examining monthly anomalies related to each phenomenon, it will be worth validating the steadiness of the correlation on a monthly basis. Figure 1 shows the simultaneous correlation coefficients between those indices during 1950–2000 for each month from October to April. The correlation is significant at the 95% level for all months displayed, but is lower (higher) than the correlation based on a seasonal mean (December–February) time series during the early (late) winter. The maximum appears in February when the correlation reaches +0.89, suggesting that the NAO anomalies in this month reveal a wider spatial extent than those in other winter months.

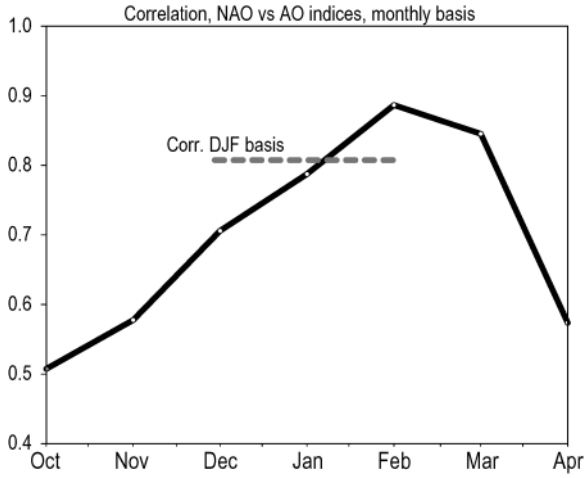

FIG. 1. Correlation coefficient between the NAO and AO indices for each month. Correlation using the winter Dec–Feb (DJF) mean time series is indicated by a dashed line.

a. Downstream extension of the NAO

Monthly NAO anomalies in the 300-hPa geopotential height and 925-hPa temperature from December to February are presented in Fig. 2, together with the corresponding AO anomalies. Among these anomaly maps a common feature is found over the Atlantic and surrounding regions: north–south dipole in the height anomalies that characterizes the NAO, low-level warming over the eastern half of the United States and Scandinavia, and cooling over the Labrador Sea and northern Africa. The AO anomalies reveal another center over the North Pacific where positive height anomalies extend from East Asia, which is connected with the low-level warming over the region through the hydrostatic constraint (Figs. 2d–f). It is this pattern of the AO that has been recognized as the hemispheric variability. On the other hand, the NAO anomalies in December are confined to the Euro–Atlantic sector as they match the regional nature of the NAO (Fig. 2a). It should be noted, however, that the NAO anomalies in February show a wider horizontal structure that is quite similar to the AO anomalies (Fig. 2c). This ''downstream extension'' of the NAO is subtle in January (Fig. 2b) but clear in March as well (not shown), consistent with the high correlation between the AO and NAO indices during the months (Fig. 1). The similarity between Figs. 2c and 2f indicates that there exist NAO-covariant interannual fluctuations over East Asia and the North Pacific during a certain month, contrasting with previous arguments that point out the lack of such an interbasin connection associated with the AO/NAO.

Month-to-month change in the interannual variability of the NAO has also been reported by Barnston and Livezey (1987). Hurrell (1996) shows that the NAO has the largest influence on the hemispheric surface temperature variance among various teleconnection patterns. It turns out from Fig. 2 that the influence was

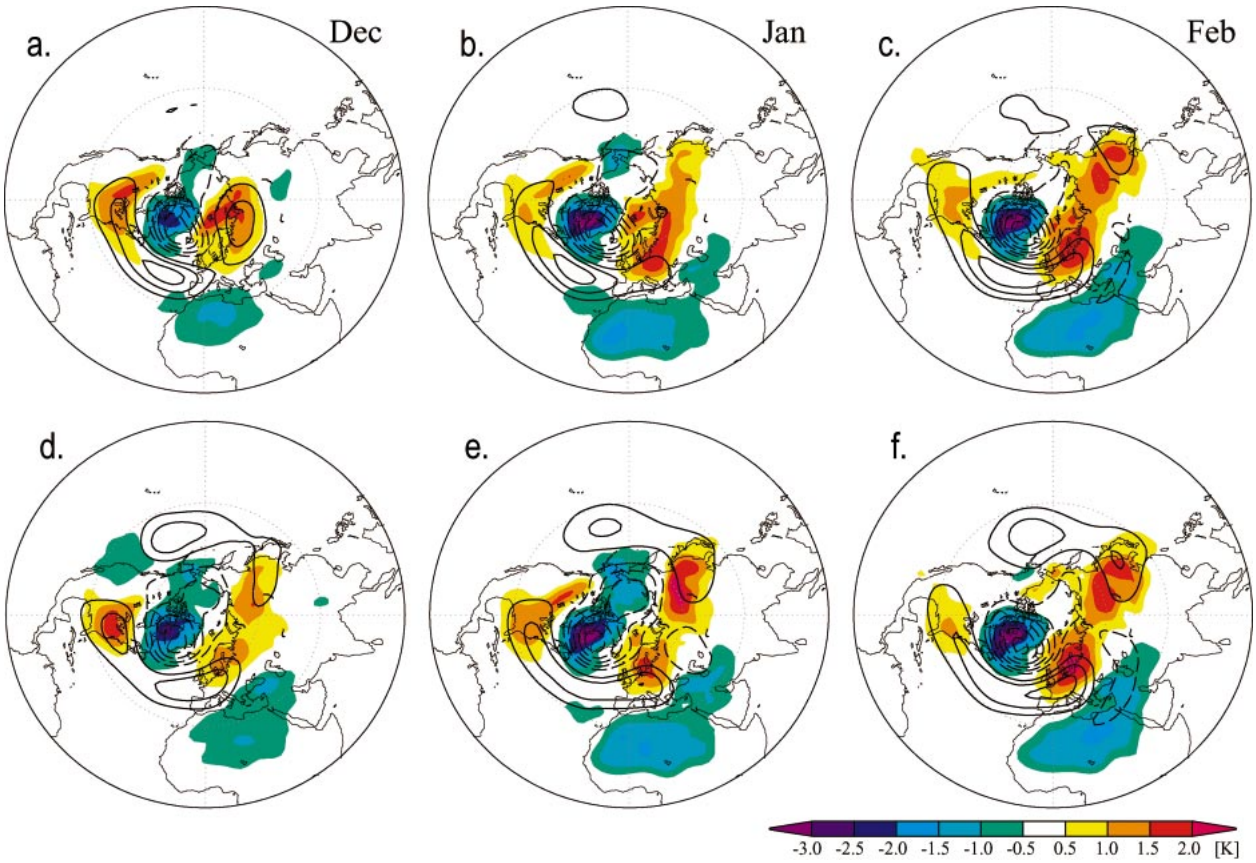

FIG. 2. (a)–(c) Monthly mean anomalies in 300-hPa geopotential height (contour) and 925-hPa temperature (color) from Dec to Feb, respectively, regressed onto the monthly NAO index. The contour interval is 20 m while negative contours are dashed (the zero contour omitted). (d)–(f) As in (a)–(c) but for regressed anomalies onto the AO index.

mainly due to the downstream extension occurring in late winter. Then, how can the NAO induce the near-surface warming over a wide area of Eurasia? A process which likely happens is horizontal temperature advection, more specifically the zonal advection of the climatological temperature gradient by the anomalous zonal-mean zonal wind. With respect to the AO, Thompson and Wallace (2000) depict that this advection term generates an anomalous temperature tendency quite similar to the low-level temperature anomaly pattern shown in Figs. 2d–f. For example, the zonal-mean wind associated with the positive phase of the AO (cf. Fig. 2d) shows an enhanced westerly around 55°N, which advects warm climatological temperature over the Atlantic Ocean deeper into the Eurasian continent. It is well known that the pronounced zonally uniform components characterize the AO, and dynamical modeling work suggests the AO-like structure originated by a coupling between zonal-mean anomalies and the climatological zonal asymmetry, which involves the aforementioned temperature advection (Ting et al. 1996; DeWeaver and Nigam 2000; Kimoto et al. 2001; Watanabe and Jin 2004).

The anomalous zonal-mean wind associated with the NAO has a meridional profile nearly identical to that associated with the AO except for slightly smaller magnitude (not shown). Nevertheless, low-level temperature anomalies in the NAO regressions are confined, compared to the AO anomalies, to early winter, suggesting that the advection due to anomalous zonal-mean zonal wind is not a unique process that brings the near-surface warming over Eurasia although it does work (Xie et al. 1999). We explore another possibility for the temperature anomalies: an upper-level circulation anomaly that is dynamically induced, which balances the temperature field beneath. Since the January fields exhibit a mixture of December and February anomalies in terms of the downstream extension (Fig. 2b), a comparison is made in the following analysis between December and February anomaly maps in order to distinguish the NAO without and with the downstream extension.

As noted above, the AO/NAO-covariant circulation anomaly has a substantial projection on the zonally uniform field. The anomalous circulation as indicated by the zonal wind or the streamfunction anomalies often masks the regional feature because of their pronounced zonal mean components. Therefore we analyze the circulation anomalies as represented by the meridional

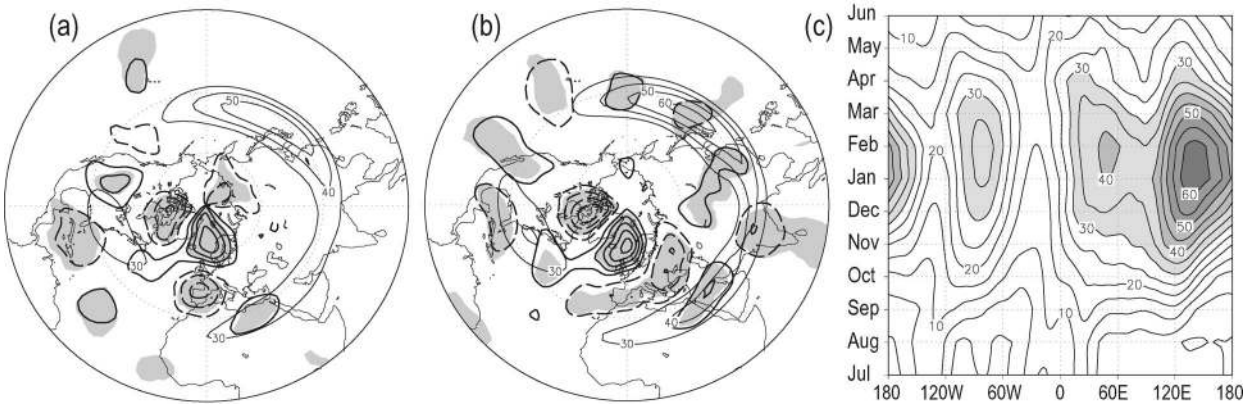

FIG. 3. Monthly mean anomalies in 300-hPa meridional wind (thick contour) regressed onto the monthly NAO index in (a) Dec and (b) Feb. The contour interval is 1 m s^{-1} while the anomalies significant at the 95% level are shaded. Superimposed is the climatological zonal wind at 300 hPa (thin contour) with the interval of 10 m s^{-1}. (c) Time–longitude section of the 300-hPa climatological zonal wind along 30°N. The contour interval is 5 m s^{-1}.

wind, which may be a good indicator for the zonally asymmetric teleconnection patterns (cf. B02).

Figures 3a and 3b show the monthly NAO anomalies in the 300-hPa meridional wind in December and February, respectively. It is evident that the meridional wind anomalies are mostly confined to the Atlantic region in December whereas they extend to the entire midlatitude band in February. The anomalous northerly and southerly wind near Greenland corresponding to the deepened Icelandic low is similarly found in both regression maps. In February, they are continuous toward the Middle East besides emanating to East Asia and the North Pacific along the axis of the subtropical jet (thin contours in Fig. 3b). Such a zonally oriented wave train is identified as one of the dominant teleconnection patterns at subseasonal time scales (Kushnir and Wallace 1989; B02). B02 further interprets the pattern shown in Fig. 3b as quasi-stationary Rossby waves trapped on the Asian jet, which acts as waveguide (Hoskins and Ambrizzi 1993). Although it should be again emphasized that the anomalous meridional wind in Fig. 3b is found on interannual time scale, analysis in the next section shows that it does happen on an intraseasonal time scale as well. The climatological zonal wind at 300 hPa along 30°N (Fig. 3c) illustrates a seasonal evolution of the Asian jet around 60°E which is weaker in early winter and strongest in February. Thus the February basic flow may provide more favorable conditions than that in December in terms of the establishment of the Asian jet waveguide.

b. Anomalous Rossby wave source

Since the wave train in Fig. 3b is quite similar to the ''waveguide pattern'' found by B02 and, furthermore, it has an equivalent barotropic nature (not shown), processes that generate the anomalies are conceivably understood in a barotropic vorticity equation. For this purpose, the Rossby wave source is computed following Sardeshmukh and Hoskins (1988):

$$S = -\nabla \cdot (\mathbf{v}_\chi \xi), \tag{2}$$

where $\xi \equiv \zeta + f$ is the absolute vorticity while $\mathbf{v}_\chi$ is the divergent wind vector calculated from the velocity potential field. Note that the wave source S is computed by means of monthly mean fields so that it excludes a contribution from submonthly perturbations. As in the other variables, the anomalous S is regressed upon the NAO index for each month, denoted as S'.

Figure 4 displays S' at 300 hPa associated with the NAO in December and February, respectively, superimposed on the climatological mean zonal wind. The anomalous Rossby wave sources are similar to each other over the Atlantic basin, namely, positive and negative sources to the west and east of Greenland, positive anomaly around the Azores and negative anomaly on the equatorial band. However, conspicuous differences are found over continents from Africa to East Asia. While few significant anomalies are observed in December, there are a number of significant anomalies along the Asian jet in February. In particular, S' over southern Europe to the Middle East appears to dominate the others, and it is the region where the Asian jet is established.

The anomalous Rossby wave source in Fig. 4 can be decomposed into several terms, each of which is calculated from monthly NAO anomalies as

$$S' = \underbrace{-\nabla \cdot (\overline{\mathbf{v}}_\chi \zeta')}_{S'_1} \underbrace{-\nabla \cdot (\mathbf{v}'_\chi \overline{\zeta})}_{S'_2} \underbrace{-\nabla \cdot (f\mathbf{v}'_\chi)}_{S'_3} - \nabla \cdot (\mathbf{v}'_\chi \zeta'), \tag{3}$$

where the primes denote anomalies regressed upon the NAO index while overbars are climatological quantities. The anomaly is not so huge that the nonlinear term can be neglected, then we can specify the leading term be-

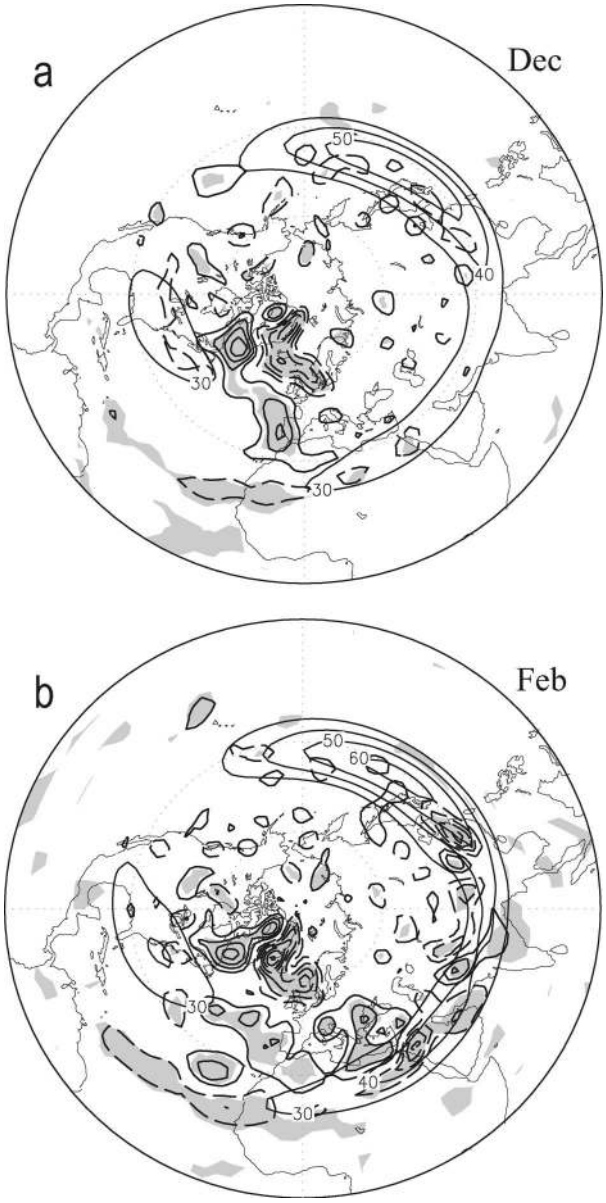

FIG. 4. As in Figs. 3a,b but for the Rossby wave source anomalies, S'. The contour interval is 2×10^{-11} s^{-2}.

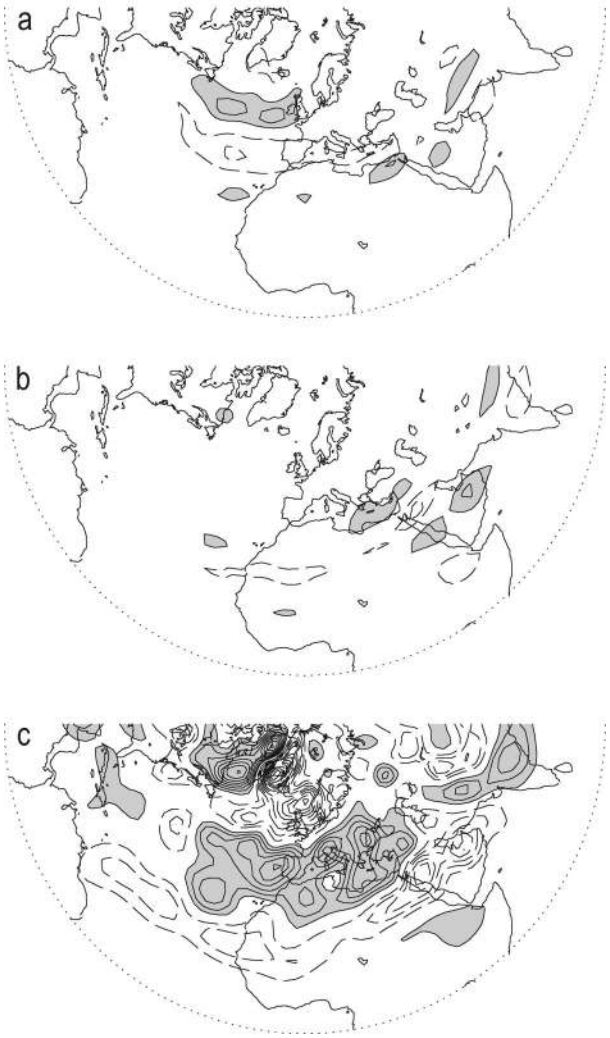

FIG. 5. As in Fig. 4b but for the linearized components: (a) S'_1, (b) S'_2, and (c) S'_3 as defined by Eq. (3). Note that the contour interval is 1×10^{-11} s^{-2} and shading denote positive anomalies greater than 1×10^{-11} s^{-2}.

tween S'_1 and S'_3 resulting in S' shown in Fig. 4b. The three terms are illustrated in Fig. 5, with a denser contour interval than in Fig. 4. Note that their sum is nearly identical to Fig. 4b. It is obvious that the first two terms (Figs. 5a,b), the convergence associated with the relative vorticity, are less dominant than the third term (Fig. 5c), which is mostly the same as a commonly used divergent forcing, $-fD'$ (e.g., Branstator 1985), where D' is the divergence anomaly. Sardeshmukh and Hoskins (1988) notice that one should correctly evaluate the Rossby wave source using Eq. (4) but not by a simple $-fD'$ term in order for accurate diagnosis of the rotational flow. In the present case, however, the $-fD'$ approximation seems valid, which tells us that most of the anomalous Rossby wave source in Fig. 4b comes directly from the divergence anomaly associated with the NAO. In the subsequent section, diagnoses using the linear barotropic model are made for the Rossby wave source and circulation anomalies associated with the NAO.

c. Steady solutions in a barotropic model

Regressed NAO anomalies in February showing the zonally oriented wave train along the Asian jet (Fig. 3b) concurrent with the anomalous Rossby wave source near the jet entrance region (Fig. 4b) suggest that the downstream extension of the NAO is accomplished by energy propagation due to stationary Rossby waves excited by the vorticity source, perhaps, associated with

the NAO. This inference is encouraged by a theoretical consideration of the Rossby wave reflection (Hoskins and Ambrizzi 1993), which depicts that the region where the meridional gradient of the absolute vorticity, $\partial\bar{\xi}/\partial y$, is large, and hence stationary wavenumber K_s is also large, tends to trap stationary Rossby waves. Because of the meridional curvature, subtropical jet streams such as the Asian jet have local maxima in K_s and therefore act as waveguides for quasi-stationary Rossby waves. Following this theory, the vorticity source around the Mediterranean Sea and Middle East may be capable of exciting quasi-stationary waves with a zonal wavenumber larger than K_s, which is roughly 5–7 along the winter Asian jet.

In this section, by means of a barotropic model we test whether the above processes do occur. The ability of the barotropic model is first validated in terms of the reproducibility of observed NAO anomalies. By assuming that the tendency term in Eq. (1) can be neglected on the time scale discussed in this section, a steady streamfunction response is calculated with the February climatological flow as a basic state and the anomalous vorticity source depicted in Fig. 4b, then compared to the observed counterpart (Fig. 6). For both the observed and simulated streamfunction anomalies the zonal mean component has been removed in Fig. 6 so as to visualize the waveguide patterns. Since the vorticity source anomaly is less reliable in higher latitudes due to larger errors in the divergent wind, the forcing is restricted between 0° and 60°N in computing the steady response. The observed 300-hPa streamfunction anomaly in February, denoted as ψ^*_{300} (asterisk stands for the deviation from zonal average), reveals a zonally elongated pattern over most parts of the Eurasian continent whereas a wavelike feature from East Asia to the North Pacific (Fig. 6a). The steady ψ^*_{300} response with given observed S' reproduces such patterns well (Fig. 6b) although several discrepancies exist, for example, too strong anticyclonic response over the North Pacific and response to the north of the Aleutian Islands with sign opposite to the observation. These shortcomings must be caused by the following reasons: lack of the forcing due to submonthly Rossby wave source anomalies, steady state assumption, errors in high-latitude vorticity source, and simple representation of nonlinear dissipation included by the linear damping, in which the first two may be the principal causes. Nevertheless, the overall feature in Fig. 6b is similar enough to the observed anomalies in Fig. 6a, indicating that the barotropic model is capable of simulating the NAO-covariant circulation anomalies over Eurasia. It should be noted that the NAO pattern itself is not well reproduced in the steady response due to lack of transient eddy vorticity forcing, which has been shown to be dominant in driving the NAO pattern (cf. Hurrell and van Loon 1997; Feldstein 2003).

The barotropic response captures two anomalous ridges over East Asia and the North Pacific, which accompany a wave train in the meridional wind as observed (not shown, but similar to Fig. 3b). A question is raised here: which part of the Rossby wave sources in Fig. 4b is most responsible for the downstream response? To answer the question it is useful to employ the so-called Green's function approach as introduced by Branstator (1985). Namely, we define the Green's function as

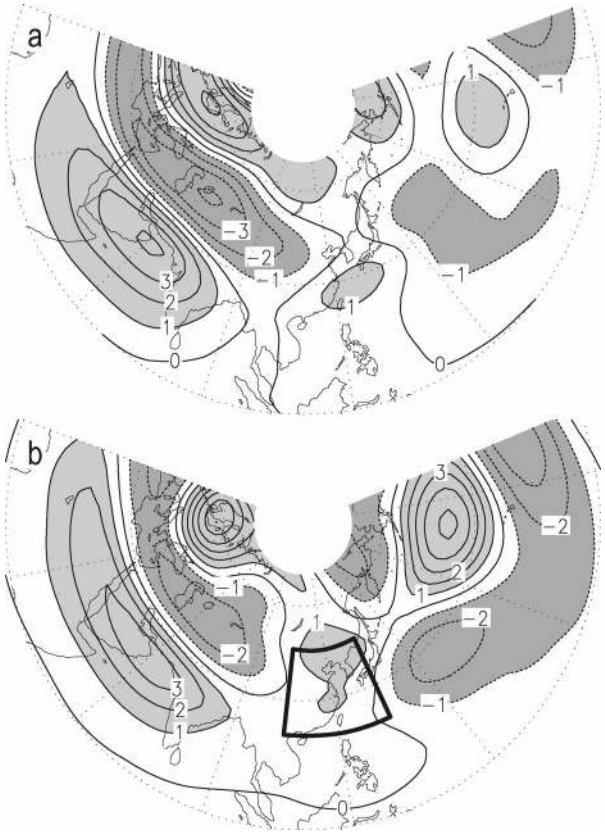

FIG. 6. (a) Monthly mean anomalies in 300-hPa streamfunction (zonal mean removed) in Feb, regressed onto the Feb NAO index. The contour interval is 1×10^6 m^2 s^{-1} while the anomalies greater (less) than -1×10^6 m^2 s^{-1} are light-shaded (dark-shaded). (b) Steady streamfunction response in a barotropic model forced by the vorticity source shown in Fig. 4b. A thick rectangular box indicates the target region for the optimal vorticity source (see text).

$$G(\lambda, \varphi, \lambda', \varphi') = \mathcal{L}^{-1}\delta(\lambda, \varphi, \lambda', \varphi'),$$

$$\delta = \begin{cases} f_0 & \text{for } \lambda = \lambda', \varphi = \varphi' \\ 0 & \text{elsewhere,} \end{cases} \quad (4)$$

where λ and φ are longitude and latitude, respectively. The linearized operator of the model, that is, the left-hand side of Eq. (1), with the tendency term neglected, is symbolically represented by $\mathcal{L}$ and the function G is obtained as a steady vorticity response to the forcing δ, which is a delta function having the value f_0 only at $\lambda = \lambda'$ and $\varphi = \varphi'$. The forcing position is actually given on discretized grid points corresponding to the T42 horizontal resolution, then G consists of $128 \times 32 = 4096$ steady response patterns (no forcing over the Southern

Hemisphere). We set $f_0 = 1 \times 10^{-10}$ s^{-2} multiplied by sin φ to mimic the divergent forcing that dominates in S' (Fig. 5).

Green's function, which depends not only on space but also on the forcing position, is now used to evaluate an *optimal vorticity source* for a specific streamfunction response. Given a target region denoted as T, the optimal source S_o is defined as

$$S_o(\lambda', \varphi') = \frac{1}{\sigma}\left(\frac{1}{A}\int_T \nabla^{-2}G\right), \tag{5}$$

where A is the area extent of the target region and the integral is taken in terms of λ and φ: S_o is obtained in a sense of the streamfunction and normalized by a factor σ such as to have unit spatial variance. We choose the anomalous ridge over East Asia as the target region, which is indicated by a rectangular box in Fig. 6b, since it is one of the major parts in the NAO downstream extension. The region is slightly more southward than the simulated anomalous ridge while it covers the observed counterpart. It is found that the result is not very sensitive to slight meridional change in the target region.

Shown in Fig. 7 are the distribution of S_o respectively evaluated with December and February basic flow, superimposed on the basic-state westerly as well as the location of T. The optimal source defined by Eq. (5) implies that the positive (negative) vorticity source at centers of positive (negative) S_o is effective in exciting the positive streamfunction response over the region T. For both December and February basic flow S_o has distinctive positive maxima over the Mediterranean Sea, Bay of Bengal, and Siberia while a minimum over the Arabian Sea. The positive values over the Mediterranean Sea are stronger in February, consistent with a stronger Asian jet to the east, which manifests that even for the same vorticity forcing over the region the East Asian ridge is more strongly excited in February, possibly due to the jet waveguide being solidly established. A comparison between Figs. 4 and 7 enables us to estimate which part of the observed Rossby wave sources associated with the NAO plays a leading role for the eastward extension. It is easily identified that the positive vorticity source over the Eastern Mediterranean Sea coincides with another in February while it is found only in S_o during December, suggesting that the anomalous wave source over the region is a key linking the NAO to anomalous circulation over East Asia. The optimal vorticity source reveals that the East Asian ridge can be excited by the subtropical forcing over the Indian Ocean and the western Pacific as well, but it is not found in S' associated with the NAO.

We also tested the sensitivity of the optimal source pattern to the choice of the target region. If the region T is defined by the average over 25°–45°N, 145°–175°E, which corresponds to the anomalous trough in Fig. 6, the optimal negative source emerges at the jet entrance where the positive source is found in Fig. 7. On the other hand, for T between 120° and 150°E, the optimal vorticity source reveals a quite similar distribution to Fig. 7 but the positive source near the Asian jet entrance is shifted eastward by 20° (not shown). This result implies that the zonal phase of the wave train as observed in Fig. 3b is determined by the position of the vorticity source but not other processes such as the zonal inhomogeneity in the time-mean flow. In fact, B02 identified a family of these wave trains, each of which has a different zonal phase, consistent with the above interpretation.

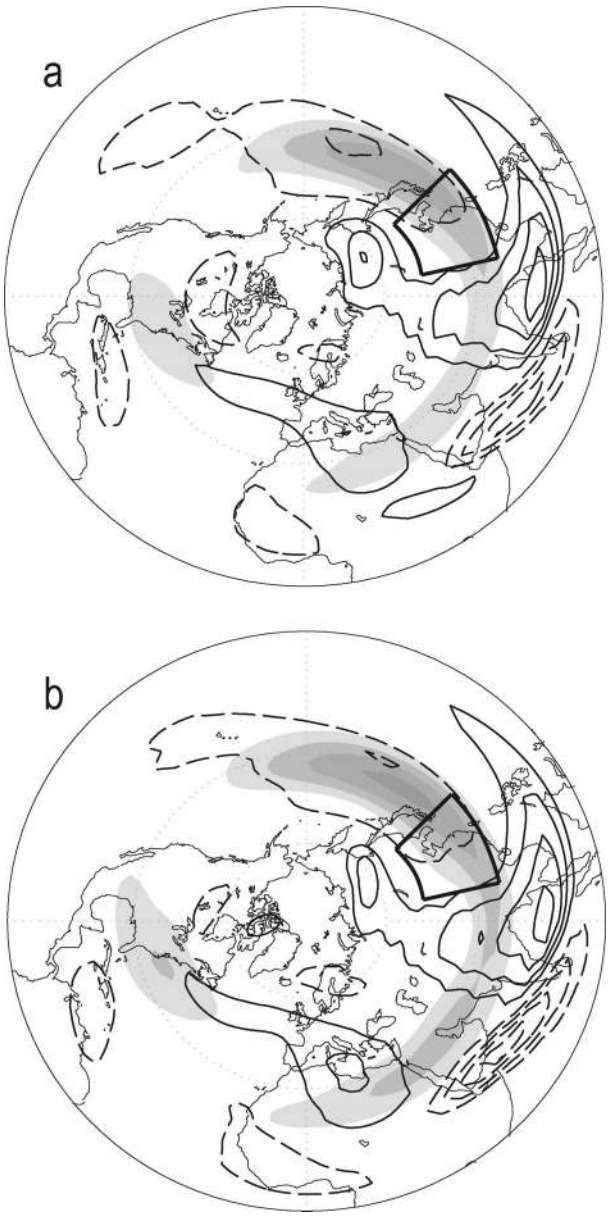

FIG. 7. Optimal vorticity source to the target region (denoted by a thick rectangular box) obtained by the barotropic model linearized about (a) Dec and (b) Feb climatological flow. The contour interval is 1 nondimensional unit. Shading indicates the climatological zonal wind in the corresponding month, as shown in Figs. 3a,b.

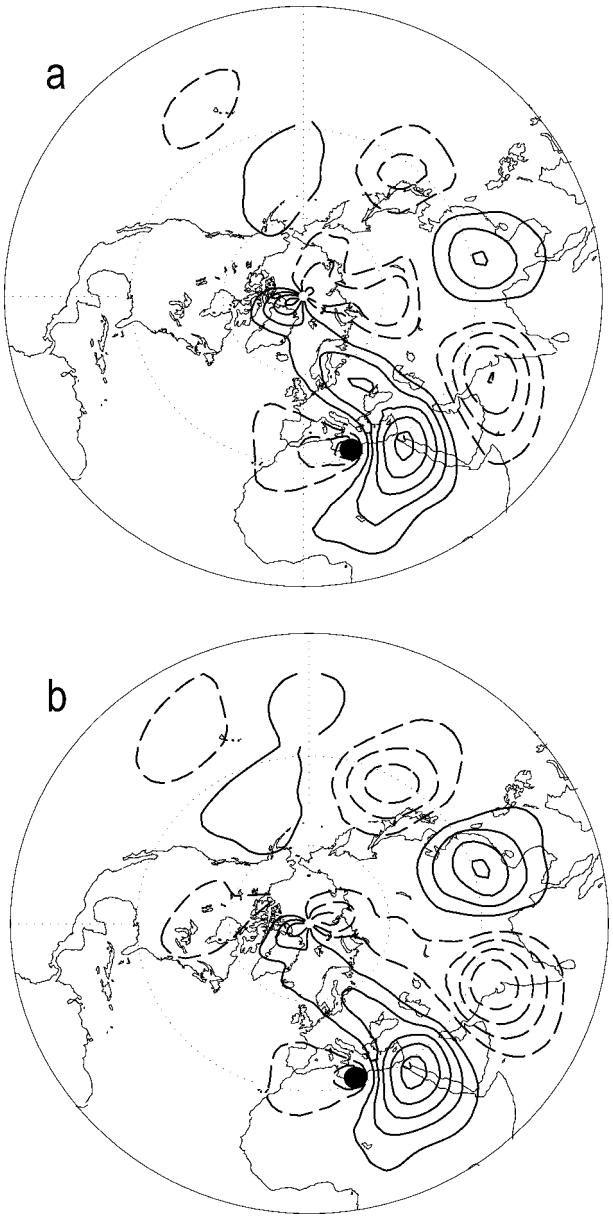

FIG. 8. Steady barotropic model response as represented by the meridional wind forced by a pointwise vorticity source over the Mediterranean Sea (denoted by a closed circle). The basic state is (a) Dec and (b) Feb climatological flow. The contour interval is 0.01 m s^{-1}.

Namely, the anomalous Rossby wave source near the Asian jet entrance, when it is produced in association with the NAO, will excite one of the waveguide teleconnection patterns attributed to the spatially fixed vorticity source.

The steady meridional wind response to the pointwise vorticity forcing placed at the center of positive S_o over the Mediterranean Sea is shown in Fig. 8. As expected, a zonally oriented wave train is excited to the east of the forcing, strictly along the Asian jet. The position of southerly and northerly wind anomalies are in remarkable agreement with those observed in February (Fig. 3b). It should be noted that the wind response in December is quite similar to that in February (Fig. 8a), indicating that the vorticity source over the Mediterranean Sea can be optimal in both months, as suggested by Fig. 7. The above diagnosis implies that the lack of the downstream extension of the NAO in December results from the lack of S' in an optimal region (cf. Fig. 4a), which is crucial for the waveguide teleconnection as shown in Fig. 8. This automatically leads to a conclusion that the stronger Asian jet in February is of secondary importance.

d. Mediterranean convergence and the NAO

In the previous subsections the convergence anomaly over the Mediterranean Sea was shown to play a key role in the NAO downstream extension. While detailed analysis of how the NAO produces the Mediterranean convergence anomaly will be performed in the next section, preliminary results are shown here. We especially focus on whether the February time mean state favors it. In other words, the NAO extremes that accompany the downstream extension are looked for in December and January as well, using an analysis other than the linear regression.

First, an index that measures the Mediterranean convergence (denoted as MC) is defined by taking the monthly convergence anomaly at 300 hPa averaged over 25°–45°N, 10°–30°E, referred to as the Mediterranean convergence index (MCI). The time series of MCI in each winter month are shown in Fig. 9, superimposed on the Hurrell (1995) NAO index. Correlation coefficients between the two indices are negligible in December ($r = 0.14$) while significantly increasing in January and February ($r = 0.39$ and $r = 0.41$, respectively), which support our hypothesis that the downstream extension appears when the MC is coherent with the NAO. It is interesting to note that the MCI is stably correlated with the AO index, ranging from $r = 0.46$ in December to $r = 0.50$ in February, which again matches the regression analysis that shows that the AO anomalies always accompany the signal over East Asia and the North Pacific (Fig. 2).

The NAO extremes can be classified into two categories by taking the concurrence of the MC into account, as summarized in Table 1. Although the NAO index and MCI are almost uncorrelated in December, about half of the positive NAO extremes as defined by the index value exceeding one standard deviation accompanies the positive phase in MCI. This ratio is roughly the same in the other winter months for the positive NAO/MCI extremes whereas the concurrence of negative NAO and MCI extremes is hardly found in December and January. While the cause of this phase asymmetry is not clear at the moment, it might result in a low correlation between the NAO index and MCI in December (Fig. 9a). The categorized statistics also suggest that the downstream

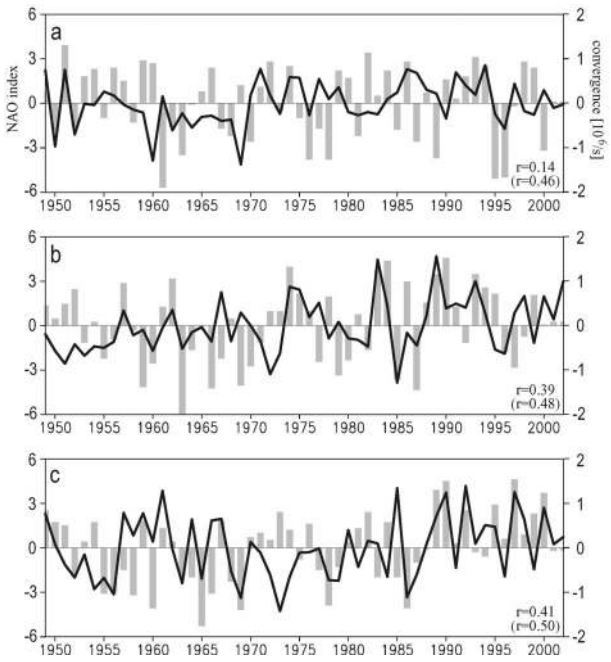

FIG. 9. Time series of Hurrell's (1995) NAO index (bars) and the Mediterranean convergence index (MCI) defined by the 300-hPa convergence anomaly averaged over 25°–45°N, 10°–30°E (lines) for (a) Dec, (b) Jan, (c) Feb. Long-term average has been removed. Correlation coefficients between the time series are also shown at the bottom right. The values in parentheses are the correlation between the AO index and MCI.

extension may be observed in December–January if we choose positive NAO extremes adequately.

In a similar manner to Table 1, monthly composite NAO anomalies that consist of 10, 8, and 9 extremely positive years in December, January, and February (cf. Table 1) are separated into two: one based on years having positive MCI and another with negative or normal MCI years. Shown in Fig. 10 are those two composite anomalies in the 300-hPa streamfunction for each month (results are similar in the 500-hPa geopotential height). Composite anomalies that accompany the positive MC anomaly (Figs. 10a–c) have some common features for each of three months, that is, anticyclonic anomalies over East Asia, the North Pacific, and the Arabian Sea in which the former two correspond to the anomalous ridges in the NAO downstream extension (cf. Fig. 6a). Anomalous cyclonic circulation also tends to occupy a wider region over the polar cap. In contrast, the positive NAO composites that do not accompany the positive MC anomaly (Figs. 10d–f) reveal a pattern varying from month to month over those regions, although large anomalies sometimes happen such as in January. Although the statistical significance of anomalies is relatively tenuous except for the Atlantic sector, which would be due to insufficient sample size, Fig. 10 clearly represents that the NAO anomalies look like the hemispheric AO anomalies when the MC anomaly is simultaneously taking place. Furthermore, the NAO

TABLE 1. Number of years that reveal positive or negative phase of the NAO as measured by the NAO index greater or less than one standard deviation. Numbers in parentheses denote years which simultaneously reveal positive or negative values, defined by the standard deviation as well, in the Mediterranean convergence anomaly as shown in Fig. 9.

Phase of the NAO	Dec	Jan	Feb
Positive	10 (4)	8 (4)	9 (5)
Negative	10 (1)	9 (1)	8 (3)

downstream extension identified in one category of the composite (i.e., Figs. 10a–c) but not in another (Figs. 10d–f), which becomes clearer in the meridional wind composites (not shown), indicates that it is not only preferred by the February climatological flow but may occur in the other winter months.

It is noted that the NAO itself shows a slightly different structure between Figs. 10a–c and 10d–f. The former has a southern part (anticyclonic anomaly) split into the upstream center over the U.S. east coast and the downstream center over Europe, whereas the latter has a center over the North Atlantic Ocean. The composite anomalies that do not accompany the MC anomaly match the classical view of the NAO in terms of a regional north–south dipole. The circulation anomalies in Figs. 10a–c form an arching structure from North America to Europe and farther downstream, suggesting energy propagation along the path that may favorably cause the anomalous convergence over the Mediterranean Sea. The difference in the NAO structure visible in Figs. 10a–c and 10d–f is somewhat consistent with Kodera and Kuroda (2003) who point out the presence of two ''modes'' over the Euro–Atlantic sector: a regional pressure seesaw between Iceland and the Azores and a hemispheric seesaw between the Mediterranean and polar regions. However, it is hard to state the anomaly patterns, such as Figs. 10c and 10f, as a different ''mode''; rather we hypothesize that their Atlantic part (i.e., NAO) is generated by a common dynamical process but with a slight difference, for example, in the forcing and the background state (e.g., Rodwell et al. 1999; Peng et al. 2002) that cannot be specified yet. This serves as a condition whether the MC anomaly, hence downstream extension, is accomplished.

4. Intraseasonal time scale, or the NAO events

As mentioned in the introduction, several recent studies tend to reemphasize the short time scale, approximately two weeks, of the dominant teleconnection patterns, including the NAO (DelSole 2001; Feldstein 2002, 2003). Given this short lifetime, it is thought to be useful that we extend our analysis to daily fields which resolve individual events and hence enable us to understand the downstream extension of the NAO in terms of basic dynamics of the NAO life cycle. Before carrying out the analysis, all daily mean fields are

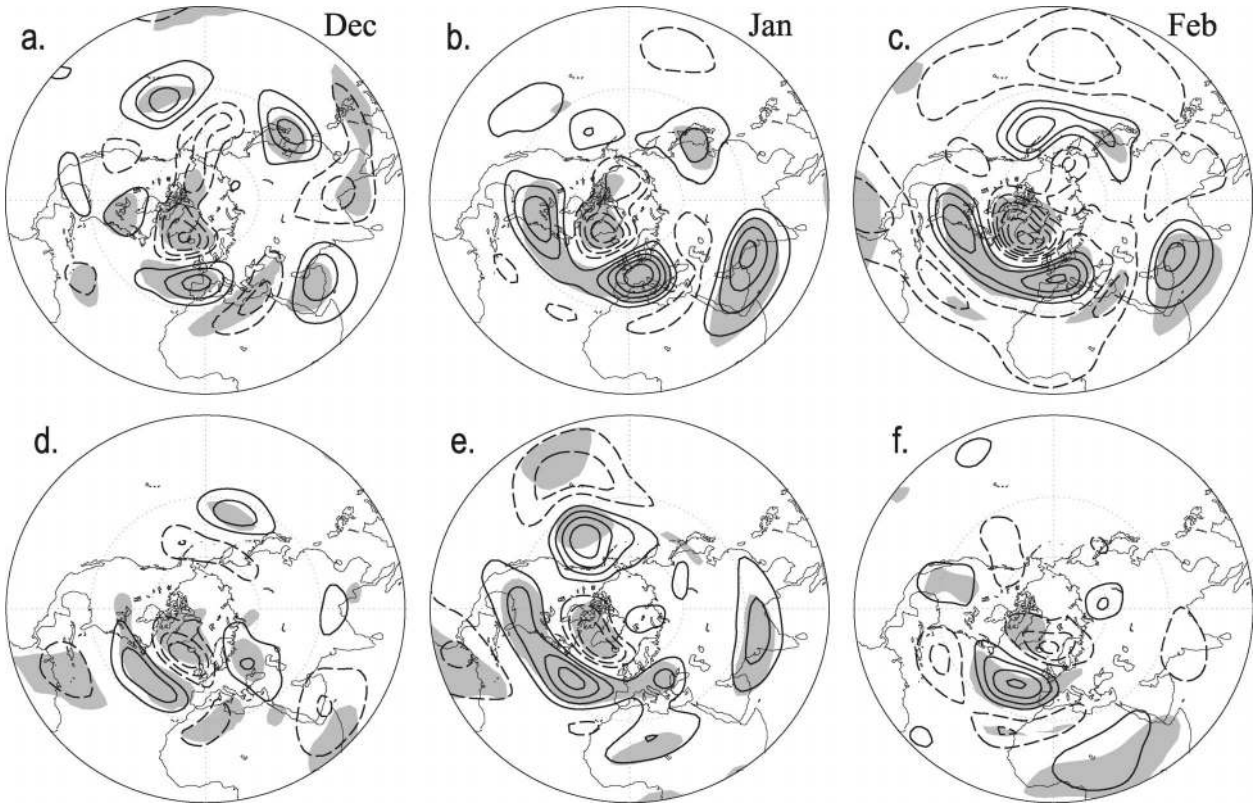

FIG. 10. (a)–(c) Monthly mean composite for the 300-hPa streamfunction anomalies in Dec, Jan, and Feb, respectively. Selected years for composite maps are those having positive values (greater than 1 std dev) both in the NAO index and MCI. The contour interval is 3×10^6 $m^2 s^{-1}$ while the shading denotes the composite anomalies significant at the 95% level. (d)–(f) As in (a)–(c) but for the composites for years having positive values only in the NAO index but not in MCI.

smoothed by a 10-day low-pass filter to remove synoptic, transient disturbances (see section 2a).

a. Detection of the NAO events

To define the NAO events we chose PC1 time series, associated with the leading EOF to daily SLP anomalies over the Atlantic sector, as an index of the NAO on an intraseasonal time scale. The leading sectorial EOF accounts for 23.8% of the total variance and clearly shows the NAO pattern (Fig. 11a). This EOF pattern, in addition to the high correlation with the canonical NAO index on an interannual time scale (cf. section 2a), allows us to consider the PC1 as a good indicator of the NAO events; therefore we refer it to as the daily NAO index hereafter. The basic property of the NAO can be represented by an autocorrelation function of the daily NAO index as shown in Fig. 11b (black line), which exhibits a decorrelation time of about six days. This is relatively short but still longer than the other EOF patterns as confirmed by the autocorrelation averaged for the leading 30 PCs (white line in Fig. 11b). If the autocorrelation function of the daily NAO index is calculated with a 31-day moving window, it is found that the decorrelation time of the NAO event is not uniform during the cold months (Fig. 11c) such that the NAO has the longest persistence in February.

The way to define the NAO events is similar to Feldstein (2002, 2003), and appears rather conventional. Namely, we define a positive (negative) episode when the positive (negative) spatial correlation between the leading EOF and daily SLP anomalies over the Atlantic sector (i.e., the EOF domain) exceeds the 99% significance level and prolong for 4 or more consecutive days. Note that the results presented in this section are not sensitive to the threshold of persistence. The peak, or mature, day of each event is determined by the highest correlation during the episode. Figures 12a and 12b indicate the positive and negative NAO events during the 1949–2002 period, respectively, following the earlier definition. The number of events are 168 and 146 for positive and negative phases of the NAO, which seem to be large enough for the composite analysis in the next section. It is interesting to note that the positive events are more frequent as well as persistent than the negative events in the recent two decades, reflecting the well-known upward trend in the NAO index.

Following the mature event dates identified in Figs. 12a and 12b we would like to perform a composite analysis to various daily, low-pass filtered fields. Given

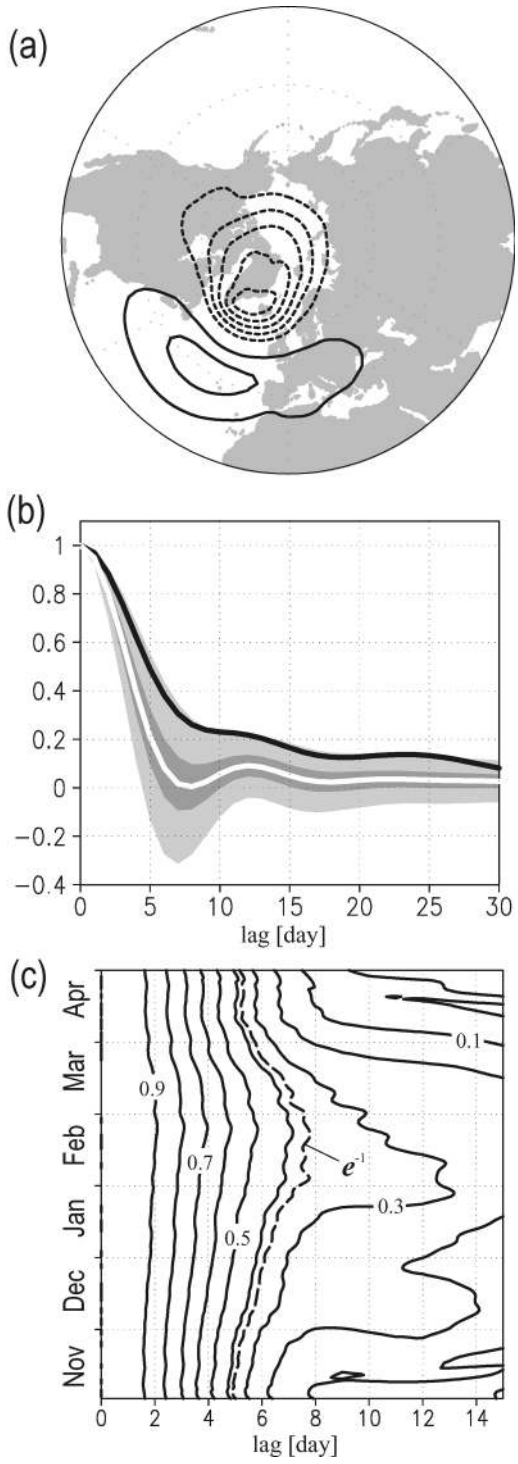

FIG. 11. (a) Leading sectorial EOF to daily, low-pass-filtered SLP anomaly, as represented by the regression of the SLP anomaly on the principal component (PC1). The contour interval is 2 hPa. (b) Autocorrelation of the PC1 time series (black line) as a function of lag in days, superimposed on average (white line), one and three standard deviations (dark and light shading, respectively) of autocorrelations for leading 30 PCs. (c) Autocorrelation of the PC1 calculated with a 31-day moving window. The contour interval is 0.1 while the dashed contour denotes decorrelation time scale.

the typical time scale of the NAO event, its time evolution will be depicted by taking 10-day lags before and after the peak day. For this purpose, the events are further selected by a criterion that, if two or more peaks are found with the interval less than 10 days, only the one that reveals the largest value is retained. This procedure consequently reduces the total number of positive and negative events to 122 and 116, respectively, as shown by Figs. 12c and 12d in which the duration of each event is made uniform at seven days for convenience. The long-term change in the persistence found in Figs. 12a and 12b, which is beyond the scope of the present analysis, has been filtered out although the decadal change in the frequency of occurrence is still visible in Figs. 12c and 12d. Since it was already shown in the previous section that the NAO downstream extension is concurrent with the upper-level convergence anomaly over the Mediterranean Sea, individual NAO events are separated into two categories by referring to the daily MCI as in section 3d but obtained from divergent field at $\sigma = 0.258$. If the MCI exceeding one standard deviation is observed during day 0–4 of an event with the same sign (i.e., positive MCI with positive NAO event), such an event is categorized into the NAO that accompanies the MC anomaly, and vice versa. The choice of day 0–4 comes from the fact that the preliminary analysis indicates, as will also be confirmed later, that a waveguide pattern in daily anomalies slightly lags the development of the NAO over the North Atlantic.

With the definition described above, it turns out that about one-third of the total events accompanies the MC anomaly, as summarized in Table 2. Frequency of concurrence of the MC anomaly with the NAO event is generally higher in the positive phase, especially during February when more than half the positive NAO accompanies the MC anomaly. This feature is consistent with the similar statistics obtained with monthly mean data (Table 1), so that pictures similar to Fig. 10 can be drawn with daily fields as well (not shown).

b. Composite analysis

Results of analysis to the monthly mean fields let us expect that the NAO events with (without) the MC anomaly reveal (do not reveal) the downstream extension as represented by the waveguide pattern over Eurasia. This inference is tested by means of the lagged composite of the low-pass filtered data in reference to the NAO events shown in Figs. 12c and 12d. The composites for the NAO with and without the MC anomaly are calculated both for positive and negative phases, but the results are quite similar to each other except for the different number of samples (Table 2) and the sign reversed, so only the anomaly patterns for positive phase are presented.

Figure 13 illustrates the time evolution of the positive NAO events in terms of the 300-hPa meridional wind

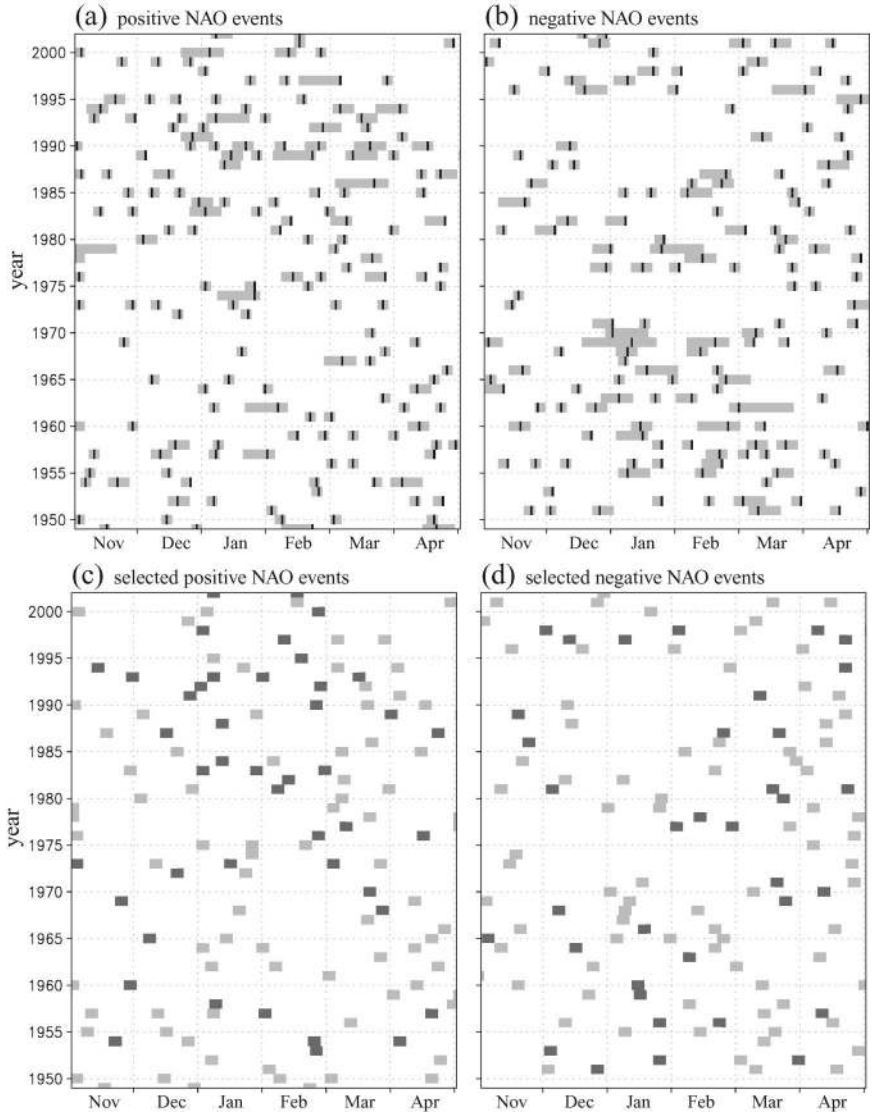

FIG. 12. (a) Positive and (b) negative NAO events identified with the leading EOF pattern (see text for the definition of the NAO events). Gray bar and black mark indicate duration and peak day of the individual event, respectively. (c)–(d) As in (a)–(b) but for selected positive and negative events. Black (gray) bars denote NAO events which accompany (do not accompany) positive and negative MCI values, respectively, exceeding one standard deviation. The length of each bar corresponds to 7 days.

TABLE 2. Number of events that reveal positive or negative phase of the NAO as indicated in Figs. 12c,d, counted for each month. Shown in parentheses is the number of events that simultaneously reveal positive or negative values in the daily MCI.

Phase of the NAO	Nov	Dec	Jan	Feb	Mar	Apr	Nov–Apr
Positive	18 (6)	16 (6)	26 (11)	19 (14)	25 (7)	18 (4)	122 (48)
Negative	14 (3)	19 (7)	19 (7)	17 (7)	22 (6)	25 (7)	116 (37)

anomaly. Since ''day 0'' coincides with the peak of events, the evolution displayed corresponds to the decay period of the NAO event. In the NAO composite anomalies that accompany the MC anomaly (Figs. 13a–d), the waveguide pattern along the Asian jet is evident after day 2. In the counterparts that do not accompany the MC anomaly (Figs. 13e–h), however, a quadrapole pattern is found over Europe throughout the period, but no extension toward East Asia is observed. This result supports our argument based on the monthly data and, furthermore, identified that the establishment of the waveguide pattern lags the peak of the NAO by two days. Eastward propagation of wave packets associated

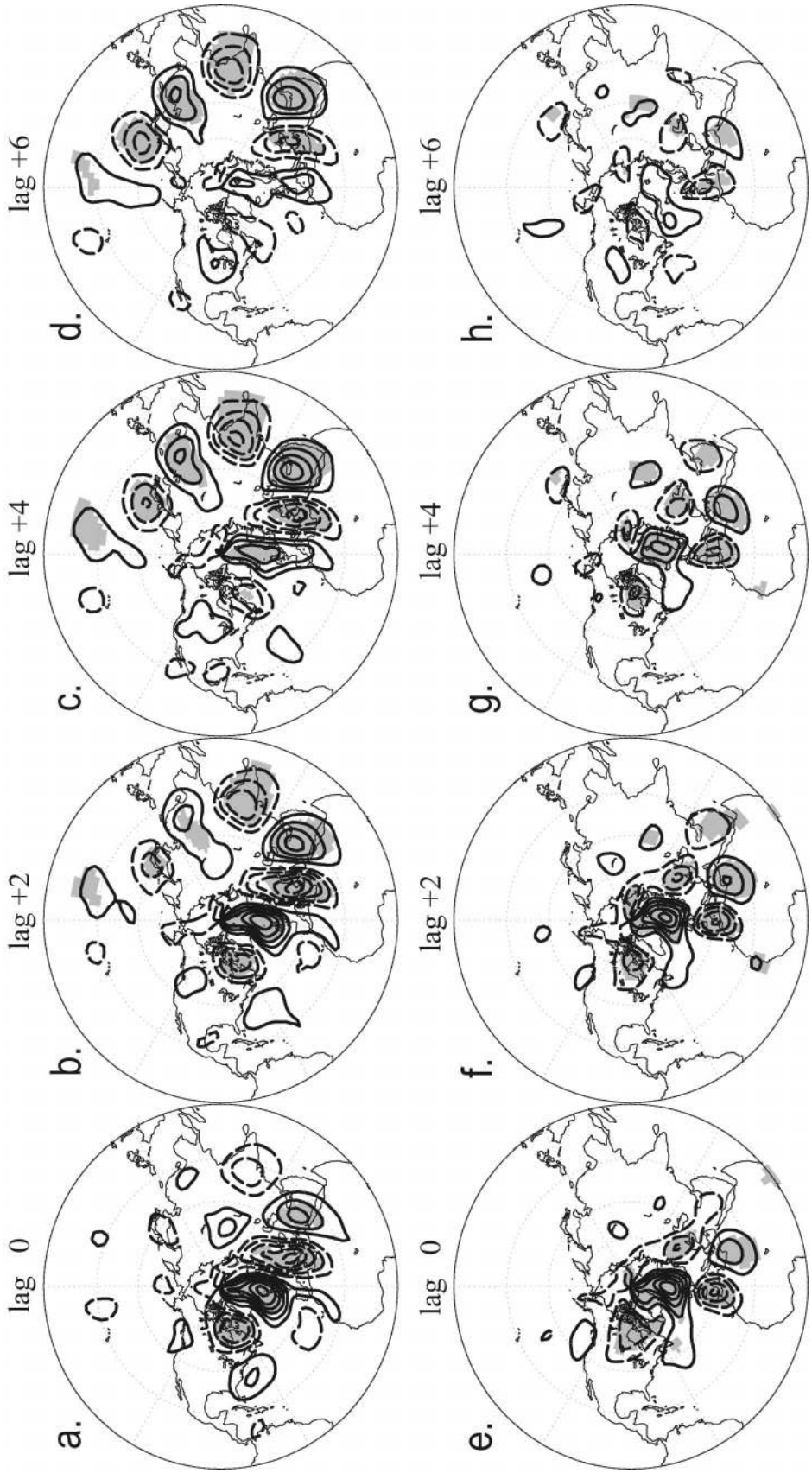

FIG. 13. (a)–(d) Composite anomalies in 300-hPa meridional wind for the positive phase of the NAO events which accompany the positive Mediterranean convergence anomaly. Lag 0 corresponds to the peak day, and subsequent anomalies at days 2, 4, and 6 are shown. Note that each event is indicated by black bars in Fig. 12c. The contour interval is 2 m s^{-1} (zero contour omitted) while shading denotes anomalies significant at the 99% level. (e)–(h) As in (a)–(d) but for the positive NAO events which do not accompany the Mediterranean convergence anomaly. These events are also shown by gray bars in Fig. 12c.

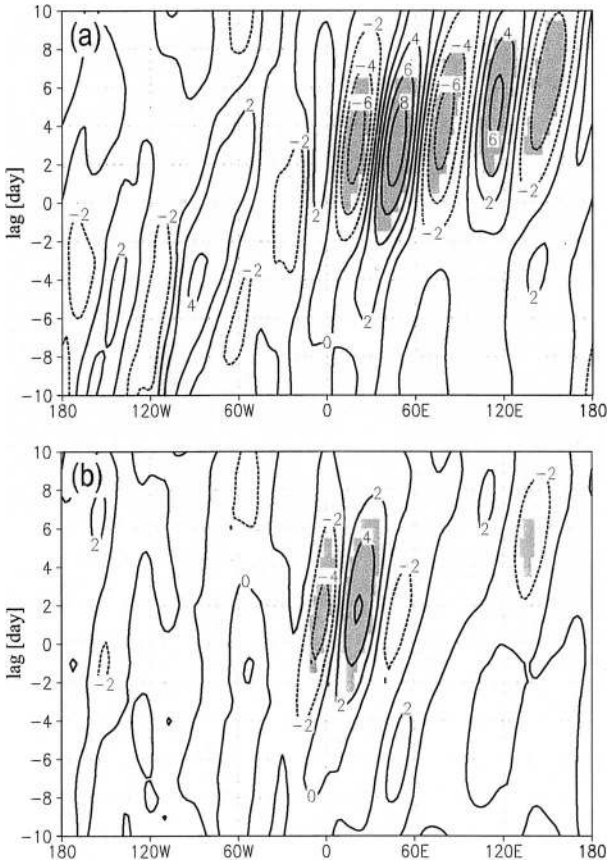

FIG. 14. As in Fig. 13 but for the longitude–time cross section at 30°N: composite for positive NAO events (a) with and (b) without the Mediterranean convergence anomaly.

with the decay period of the NAO is seen more clearly in the longitude–time section at 30°N (Fig. 14). A set of northerly and southerly wind anomalies over western Europe exists irrespective of concurrence of the MC anomaly. On the other hand, the NAO event with the MC anomaly (Fig. 14a) accompanies a fast propagation of wave packets, persistent even until day 10. These wave packets, as well as the slow phase propagation, are again consistent with the energy propagation of quasi-stationary, meridionally trapped Rossby waves (Hoskins and Ambrizzi 1993; B02). The slow phase propagation visible in Fig. 14a may be the major reason that the downstream extension can be identified in monthly mean data.

Two sets of the positive NAO composites are categorized by the MCI, so we anticipate that there are conspicuous differences in the upper-level divergent field as well (Fig. 15). In the NAO composites with the MC anomaly (Figs. 15a–d), a large positive anomaly in the velocity potential and associated convergent flows are found over the Mediterranean, which is exactly the region of optimal vorticity source in a steady limit (Fig. 7). Compared to those anomalies, the convergence signals in the counterparts (Figs. 15e–h) are weak, less persistent, and shifted to the west by about 25°. If the quasi-stationary Rossby waves in Figs. 13a–d can only be excited near the Asian jet entrance, as suggested in section 3c, the westward shift in the convergence anomaly appears crucial for the presence/absence of the NAO downstream extension. The anomalous convergence during the decay period of the positive NAO events, as shown in Fig. 15, has also been identified by Feldstein (2003) who points out, based on vorticity budgets, that the divergent term works to damp the NAO. We may therefore conclude that the NAO downstream extension is an energy dispersion accompanied by the decay of some of the NAO events. Feldstein also argues that the upper-level divergence anomaly results from the Ekman pumping near the surface. Our analysis indeed supports his argument, as revealed in Fig. 16, showing similar composites in SLP and boundary layer ($\sigma = 0.995$) divergent flows. The location of divergence (convergence) anomalies agrees well with the high (low) pressure anomalies in Fig. 16, consistent with the frictional divergent flow. Again, the NAO composite with the MC anomaly (Fig. 16a) reveals, at the peak stage, a center of positive SLP and divergence anomalies over the Mediterranean, which are not clearly detected in the counterpart (Fig. 16b). It is interesting to note that the high pressure and divergence anomalies appear over the same location, even at 5 days before the peak of the NAO (Figs. 16c and 16d) collocated with the upper-level MC anomaly (not shown), indicating that the signal of the NAO downstream extension, established during the decay stage (see Figs. 13a–d), is detectable even during the growth stage of the NAO. While thorough analysis of the whole NAO cycle is not in the scope of this study, the above results suggest as a medium-range weather forecast over East Asia that the NAO downstream extension, which affects surface temperature over the region, is to some extent predictable by carefully monitoring the developing stage of individual NAO events.

5. Concluding remarks

Motivated by the question to what extent the NAO is a regional phenomenon, this study investigated the anomalous atmospheric fields associated with the NAO on multiple time scales, using monthly and daily mean reanalysis data.

On interannual time scales, simple linear regressions upon the NAO index for each winter month reveal that circulation and temperature anomalies tend to concentrate on the Euro–Atlantic sector during early winter, which might match a classical impression of the regional NAO, whereas they extend toward East Asia and the North Pacific in late winter when anomalous ridges appear over these regions. The anomalous meridional wind was best in identifying such a hemispheric expansion, termed *the NAO downstream extension* throughout the paper, in which a zonally oriented wave train along the Asian jetstream dominates. Regressed anomalies in the

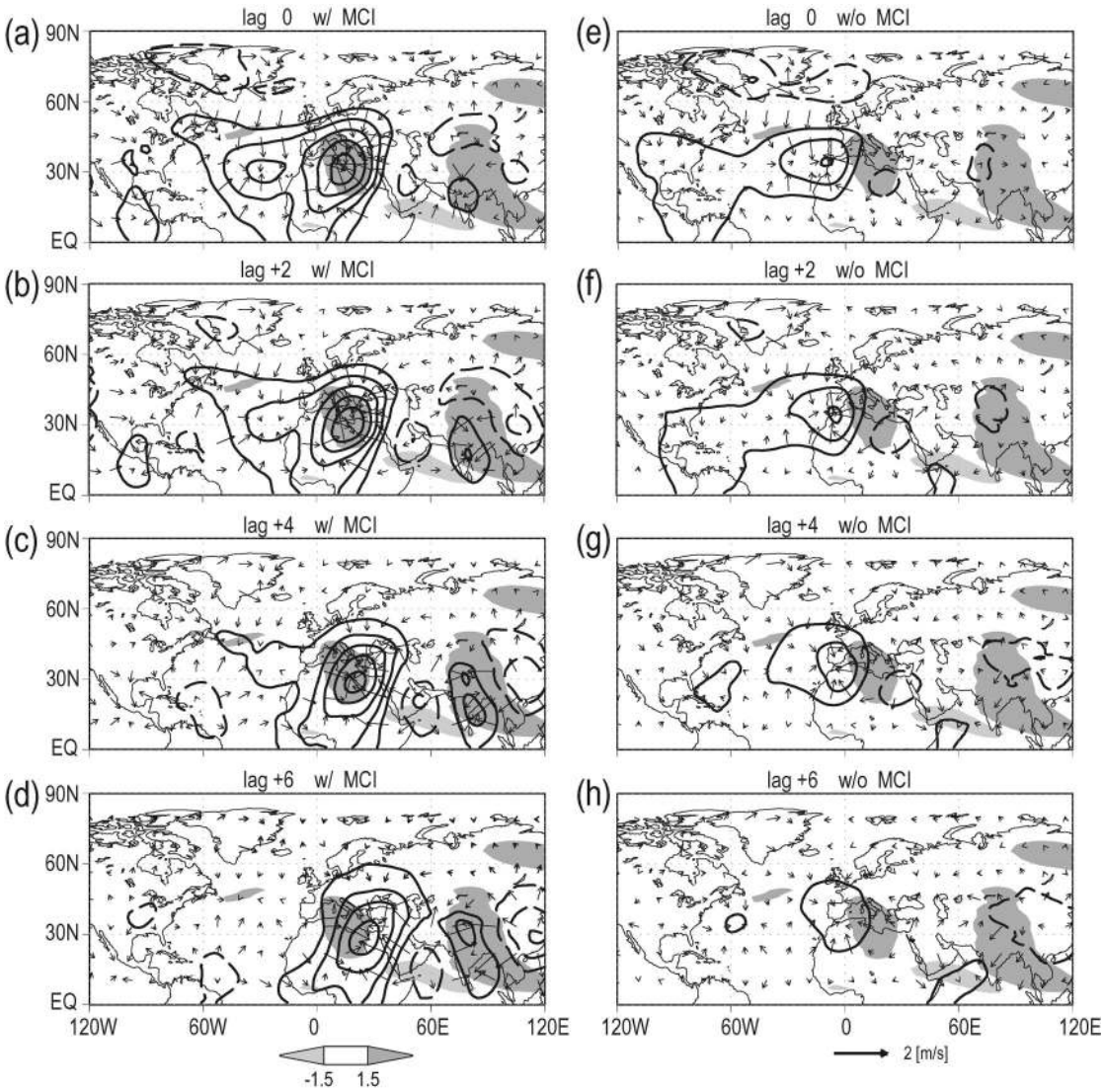

FIG. 15. As in Fig. 13 but for velocity potential (contour) and divergent wind (vector) at $\sigma = 0.258$. The contour interval is 5×10^5 m^2 s^{-1}. Dark (light) shading indicates position of the positive (negative) optimal vorticity source shown in Fig. 7.

Rossby wave source show a significant vorticity source near the jet entrance in February, mainly due to the anomalous upper-level convergence over the Mediterranean, suggesting that the downstream extension of the NAO is accomplished by quasi-stationary Rossby waves trapped on the Asian jet waveguide and excited by a vorticity source associated with the NAO. Diagnoses with the barotropic model support this idea and highlight that a positive vorticity source over the Mediterranean is optimal in exciting the wave train on the Asian jet, hence forming the anomalous ridges over the Asia–Pacific sector. It is further shown that even during December and January the downstream extension emerges when the NAO signal accompanies the Mediterranean convergence anomaly, which we conclude to be one of the key processes in linking the NAO with the East Asian Climate.

We extended our analysis to daily mean data in order to relate the downstream extension to the basic dynamics of the NAO, which actually has a relatively short time scale of about two weeks. Lagged composite analysis to the low-pass-filtered fields in reference to individual NAO events reveals that the NAO downstream extension does occur both for positive and negative phases of those events when they accompany the Mediterranean convergence anomaly, roughly accounting for half of the total number of events. We found that the wave train along the Asian jet is rapidly established about two days after the peak stage of the NAO event, indicating that the downstream extension is associated with the decay

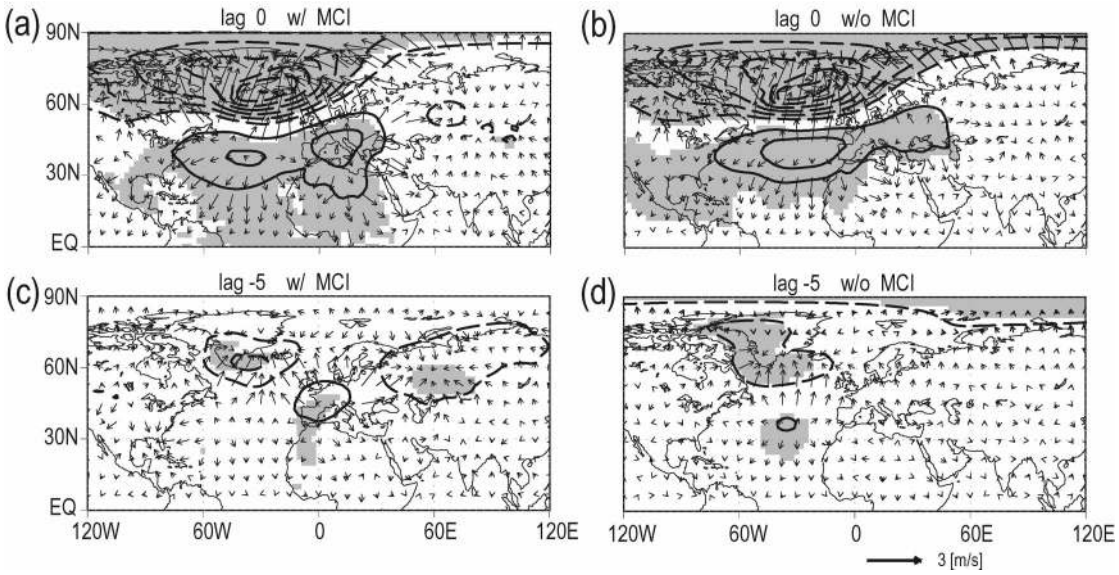

FIG. 16. As in Fig. 13 but for SLP (contour) and near-surface (at $\sigma = 0.995$) divergent wind (vector) at (a)–(b) day 0 and (c)–(d) day −5. The contour interval is 3 hPa while shading denotes anomalies significant at the 99% level.

in the NAO life cycle. It is plausible that the Mediterranean convergence anomaly results from the Ekman pumping accompanied by the southern part of surface pressure anomalies of the NAO. We thus conclude that the NAO downstream extension is probably a part of the fundamental dynamical property of the NAO itself, as schematically illustrated in Fig. 17.

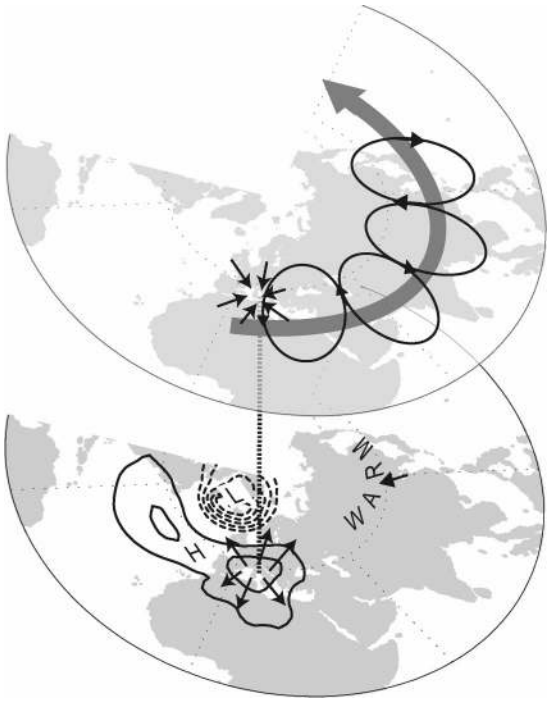

FIG. 17. Schematic illustrating the NAO downstream extension. The upper-level wave train along the Asian jet (thick arrow), which affects surface condition over East Asia, is excited by the Mediterranean convergence anomaly induced by surface frictional divergent flow (thin arrows) associated with the NAO.

Indices of the AO and NAO show the highest correlation in February, consistent with the pattern of the NAO downstream extension that is quite similar to the spatial structure of the AO. Taking this and the above results into account, the following implication is obtained for the AO/NAO debate (see introduction): a part of the AO, at least from the North Atlantic to East Asia, is interpreted as the extended NAO but not a simple combination of regional teleconnection patterns. In this regard, the hemispheric-wide structure of the AO appears to represent the physical nature in its own right, as suggested by the previous numerical studies (e.g., Kimoto et al. 2001; Watanabe and Jin 2004). On the other hand, the downstream extension is not likely to contribute to the anomalous zonal-mean zonal wind of the AO because of its zonally oriented structure. It is rather consistent with previous studies (DeWeaver and Nigam 2000; Kimoto et al. 2001) that show that the zonal-mean zonal wind anomaly of the AO mostly reflects the zonal wind anomaly over the Atlantic sector.

While the present work concentrates on the North Atlantic influence to the Asia–Pacific sector, an opposite direction of the interbasin connection has also been identified (Honda and Nakamura 2001). Interestingly, they note that the Atlantic circulation anomaly stimulated by changes in the Aleutian low over the Pacific projects well on the AO/NAO, and the connection prevails in late winter as in the NAO downstream extension. Therefore, their work and ours may cojointly indicate processes responsible to the hemispheric-scale, coherent fluctuations at work in the extratropical atmospheric circulation.

Results in section 4 of the present study also appear to have an implication for medium-range weather forecasts. While the NAO downstream extension occurs during the decay stage of the NAO life cycle, the signal of the wave source, that is, the Mediterranean convergence anomaly, is detectable during the developing stage, suggesting that the downstream extension is predictable to some extent. Since the anomalous ridge/trough associated with the downstream extension accompanies surface warming/cooling over northern East Asia (cf. Figs. 2 and 17), the Mediterranean convergence during the developing NAO may be one of the adaptive targets for the medium-range forecast in East Asian countries.

Acknowledgments. The author thanks F.-F. Jin, M. Kimoto, and H. Nakamura for stimulating discussion. Comments by two anonymous reviewers were also helpful. This work is supported by a Grant-in-Aid for Scientific Research from the Ministry of Education, Science, and Culture of Japan.

REFERENCES

Ambaum, M. H. P., B. J. Hoskins, and D. B. Stephenson, 2001: Arctic Oscillation or North Atlantic Oscillation? *J. Climate,* **14,** 3495–3507.

Barnston, A. G., and R. E. Livezey, 1987: Classification, seasonality and persistence of low-frequency atmospheric circulation patterns. *Mon. Wea. Rev.,* **115,** 1083–1126.

Branstator, G., 1985: Analysis of general circulation model sea-surface temperature anomaly simulations using a linear model. Part I: Forced solutions. *J. Atmos. Sci.,* **42,** 2225–2241.

——, 2002: Circumglobal teleconnections, the jet stream waveguide, and the North Atlantic Oscillation. *J. Climate,* **15,** 1893–1910.

Christiansen, B., 2002: On the physical nature of the Arctic Oscillation. *Geophys. Res. Lett.,* **29,** 1805, doi:10.1029/2002GL015208.

DelSole, T., 2001: Optimally persistent patterns in time-varying fields. *J. Atmos. Sci.,* **58,** 1341–1356.

Deser, C., 2000: On the teleconnectivity of the ''Arctic Oscillation.'' *Geophys. Res. Lett.,* **27,** 779–782.

DeWeaver, E., and S. Nigam, 2000: Zonal-eddy dynamics of the North Atlantic Oscillation. *J. Climate,* **13,** 3893–3914.

Dole, R. M., and N. D. Gordon, 1983: Persistent anomalies of extratropical Northern Hemisphere wintertime circulation: Geographical distribution and regional persistence characteristics. *Mon. Wea. Rev.,* **111,** 1567–1586.

Feldstein, S. B., 2000: The timescale, power spectra, and climate noise properties of teleconnection patterns. *J. Climate,* **13,** 4430–4440.

——, 2002: Fundamental mechanisms of the growth and decay of the PNA teleconnection pattern. *Quart. J. Roy. Meteor. Soc.,* **128,** 775–796.

——, 2003: The dynamics of NAO teleconnection pattern growth and decay. *Quart. J. Roy. Meteor. Soc.,* **129,** 901–924.

Honda, M., and H. Nakamura, 2001: Interannual seesaw between Aleutian and Icelandic lows. Part I: Seasonal dependence and life cycle. *J. Climate,* **14,** 1029–1042.

Hoskins, B. J., and T. Ambrizzi, 1993: Rossby wave propagation on a realistic longitudinally varying flow. *J. Atmos. Sci.,* **50,** 1661–1671.

Hurrell, J. W., 1995: Decadal trends in the North Atlantic Oscillation: Regional temperatures and precipitation. *Science,* **269,** 676–679.

——, 1996: Influence of variations in extratropical wintertime teleconnections on Northern Hemisphere temperature. *Geophys. Res. Lett.,* **23,** 665–668.

——, and H. van Loon, 1997: Decadal variations in climate assoicated with the North Atlantic Oscillation. *Climatic Change,* **36,** 301–326.

Itoh, H., 2002: True versus apparent Arctic Oscillation. *Geophys. Res. Lett.,* **29,** 1268, doi:10.1029/2001GL0113978.

Kalnay, E., and Coauthors, 1996: The NCEP/NCAR 40-Year Reanalysis Project. *Bull. Amer. Meteor. Soc.,* **77,** 437–471.

Kimoto, M., and M. Ghil, 1993: Multiple flow regimes in the Northern Hemisphere winter. Part I: Methodology and hemispheric regimes. *J. Atmos. Sci.,* **50,** 2625–2643.

——, F.-F. Jin, M. Watanabe, and N. Yasutomi, 2001: Zonal–eddy coupling and a neutral mode theory for the Arctic Oscillation. *Geophys. Res. Lett.,* **28,** 737–740.

Kodera, K., and Y. Kuroda, 2003: Regional and hemispheric circulation patterns in the Northern Hemisphere winter, or the NAO and the AO. *Geophys. Res. Lett.,* **30,** 1934, doi:10.1029/2003GL017290.

Kushnir, Y., and J. M. Wallace, 1989: Low-frequency variability in the Northern hemisphere winter: Geographical distribution, structure and time-scale dependence. *J. Atmos. Sci.,* **46,** 3122–3142.

Monahan, A. H., L. Pandolfo, and J. C. Fyfe, 2001: The preferred structure of variability of the Northern Hemisphere atmospheric circulation. *Geophys. Res. Lett.,* **28,** 1019–1022.

Peng, S., W. A. Robinson, and S. Li, 2002: North Atlantic SST forcing of the NAO and relationships with intrinsic hemispheric variability. *Geophys. Res. Lett.,* **29,** 1267, doi:10.1029/2001GL014043.

Rodwell, M. J., D. P. Rowell, and C. K. Folland, 1999: Oceanic forcing of the wintertime North Atlantic Oscillation and European climate. *Nature,* **398,** 320–323.

Sardeshmukh, P. D., and B. J. Hoskins, 1988: The generation of global rotational flow by steady idealized tropical divergence. *J. Atmos. Sci.,* **45,** 1228–1251.

Thompson, D. W. J., and J. M. Wallace, 1998: The Arctic Oscillation signature in the wintertime geopotential height and temperature fields. *Geophys. Res. Lett.,* **25,** 1297–1300.

——, and ——, 2000: Annual modes in the extratropical circulation. Part I: Month-to-month variability. *J. Climate,* **13,** 1000–1016.

Ting, M., M. P. Hoerling, T. Xu, and A. Kumar, 1996: Northern Hemisphere teleconnection patterns during extreme phases of the zonal-mean circulation. *J. Climate,* **9,** 2614–2633.

van Loon, H., and J. C. Rogers, 1978: The seesaw in winter temperatures between Greenland and northern Europe. Part I: General description. *Mon. Wea. Rev.,* **106,** 296–310.

Walker, G. T., and E. W. Bliss, 1932: World weather V. *Mem. Roy. Meteor. Soc.,* **4,** 53–84.

Wallace, J. M., 2000: North Atlantic Oscillation/annular mode: Two paradigms—One phenomenon. *Quart. J. Roy. Meteor. Soc.,* **126,** 791–805.

——, and D. S. Gutzler, 1981: Teleconnections in the geopotential height field during the Northern Hemisphere winter. *Mon. Wea. Rev.,* **109,** 784–812.

——, and D. W. J. Thompson, 2002: The Pacific center of action of the Northern Hemisphere annual mode: Real or artifact? *J. Climate,* **15,** 1987–1991.

Watanabe, M., and F.-F. Jin, 2004: Dynamical prototype of the Arctic Oscillation as revealed by a neutral singular vector. *J. Climate,* **17,** 2119–2138.

Xie, S.-P., H. Noguchi, and S. Matsumura, 1999: A hemispheric-scale quasi-decadal oscillation and its signature in northern Japan. *J. Meteor. Soc. Japan,* **77,** 573–582.